Generation of cascaded four-wave-mixing with graphene-coated microfiber

Y. Wu,[1,5] B. C. Yao,[1] Q. Y. Feng,[1] X. L. Cao,[1] X. Y. Zhou,[1] Y. J. Rao,[1,6] Y. Gong,[1] W. L. Zhang,[1] Z. G. Wang,[2,3] Y. F. Chen,[2] and K. S. Chiang[1,4]

[1]Key Laboratory of Optical Fiber Sensing and Communications, Education Ministry of China, University of Electronic Science and Technology of China, Chengdu 610054, China
[2]State Key Laboratory of Electronic Thin Films and Integrated Devices, University of Electronic Science and Technology of China, Chengdu 610054, China
[3]Interdisciplinary Nanoscience Center (iNANO), Aarhus University, Aarhus C DK-8000, Denmark
[4]Department of Electronic Engineering, City University of Hong Kong, Kowloon, Hong Kong, China
[5]e-mail: wuyuzju@163.com
[6]e-mail: yjrao@uestc.edu.cn

Received January 6, 2015; revised February 28, 2015; accepted February 28, 2015; posted March 2, 2015 (Doc. ID 231477); published March 27, 2015

A graphene-coated microfiber (GCM)-based hybrid waveguide structure formed by wrapping monolayer graphene around a microfiber with length of several millimeters is pumped by a nanosecond laser at ~1550 nm, and multi-order cascaded four-wave-mixing (FWM) is effectively generated. By optimizing both the detuning and the pump power, such a GCM device with high nonlinearity and compact size would have potential for a wide range of FWM applications, such as phase-sensitive amplification, multi-wavelength filter, all-optical regeneration and frequency conversion, and so on. © 2015 Chinese Laser Press

OCIS codes: (190.4223) Nonlinear wave mixing; (160.4670) Optical materials; (310.2790) Guided waves.
http://dx.doi.org/10.1364/PRJ.3.000A64

1. INTRODUCTION

Graphene has attracted worldwide interest for its exceptional electronic and photonic properties [1,2]; it has a unique band-gap structure, its Fermi level of graphene is tunable, its photon absorption is saturable, and its refractive index is adjustable [3–5]. Accordingly, a variety of graphene-based photonic devices have been reported, e.g., optical modulators [6,7], optoelectronic converters [8–10], ultrafast photonic lasers [11,12], highly sensitive sensors [13], and so on. Moreover, as graphene is so thin, it could be convenient to combine it with other dielectric waveguides, i.e., silicon/polymer waveguides and fibers [7,14,15].

Four-wave-mixing (FWM), especially cascaded FWM, is widely applied in modern optics, such as multi-wavelength laser, optical parametric amplification, dispersion compensation, super continuum, and comb filter [16–19]. As graphene has the unique merit of possessing ultrahigh nonlinearity especially 3-order nonlinearity over a broad spectral range [20–23], it is naturally adaptable for FWM [24,25]. Recently, by depositing graphene on silicon cavity, covering graphene on optical fiber ferule, and attaching graphene on microfiber, the generation of FWM was observed [26–30]. However, to obtain graphene-induced effective FWM is still challenging, because the interaction between graphene and transmitting light is limited, the transmission loss is significant, and the dispersion is hard to optimize.

In this paper, by using a graphene-coated microfiber (GCM), we demonstrated effective multi-order cascaded FWM based on a graphene/microfiber hybrid waveguide, for the first time (to our knowledge). By utilizing a high-power pulsed laser as pump at ~1.55 μm and a tunable CW signal light, we experimentally achieved tunable cascaded FWM with a large spectral range over 15 nm. In the FWM, the detuning was tuned from 0 to 5 nm, with a conversion efficiency up to −20 dB. Moreover, by investigating the response of the GCM in time-domain, FWM-induced multi-wavelength beating is verified. Such a GCM structure would be easily integrated into fiber-based devices and systems for generation of FWM.

2. STRUCTURE AND FABRICATION OF THE GCM

The schematic diagram of this hybrid waveguide structure is shown in Fig. 1(a). First, we use a microfiber with the diameter of sub-wavelength. Then, a monolayer of p-doped graphene is coated around the microfiber by wet-transfer method, to form the GCM. The principle of FWM induced in the GCM is shown in Fig. 1(b) [31]. When a pump light with frequency of ω_P and a signal light with wavelength of ω_S are launched into the GCM simultaneously, due to the photon absorptions and releases, electronic transitions in graphene would occur, hence generate a new frequency $\omega_E = 2\omega_P - \omega_S$. When the generated light is strong enough, cascaded FWM process would be obtained with generating higher-order harmonics, with frequency of $3\omega_P - 2\omega_S$, $4\omega_P - 3\omega_S$, and so on.

In the experiment, the silica microfiber is fabricated from a standard single-mode fiber (SMF; 28e, Corning) by chemical-etching method. A section of SMF was soaked in hydrofluoric acid for ~43 min, after that washed by DI water and ethanol alternately. Then it turned into a microoptical fiber with

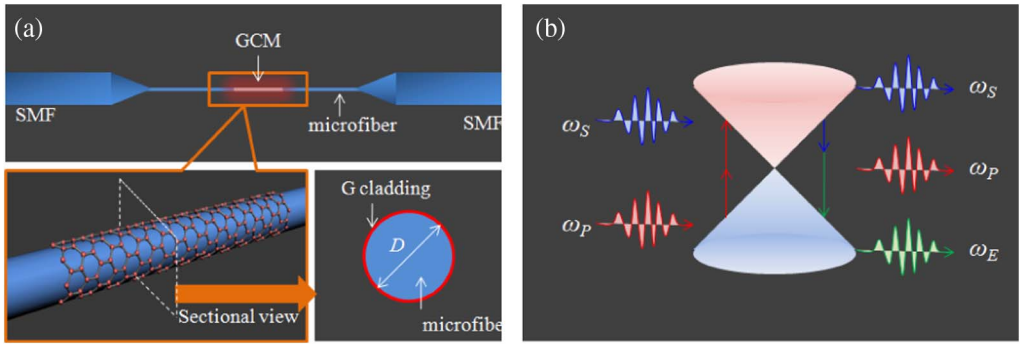

Fig. 1. (a) Schematic diagram of the GCM, in which graphene is wrapped around the microfiber with diameter of D; (b) FWM principle of the graphene.

~5 μm in diameter and ~1 cm in length. The graphene layer was grown on Cu foil by chemical-vapor deposition (CVD) method under 1000°C. It was p-doped during the wet transferring process, and finally warped around the microfiber via micromanipulation [32]. It has been verified that the linear loss of the p-doped graphene is very low and the one-photon interband transition could be suppressed [29,33], which is helpful for FWM excitation under an ultralow pump power. Figure 2 presents the images of a typical GCM sample. Figure 2(a) shows the photograph of the GCM with a 633 nm light guided through it. Correspondingly, Figs. 2(b) and 2(c) present the optical microscope of the GCM with and without 633 nm light launched. In the microscopes, visibly strong scattering at the graphene-cladded area is induced by the evanescent field enhancement of graphene. Figure 2(d) shows the scanning electron microscopy (SEM) image of the GCM, in which the fords of the graphene-clad could be seen. In Figs. 2(b)–2(d), the bar is fixed 10 μm. Figure 2(e) illustrates the Raman spectra measured at the graphene wrapped areas. The ~0.5 G-to-2D intensity ratio and the narrow full-width half-maximum (FWHM) of the G peak at verify the graphene is of high quality [34].

3. MEASUREMENT AND ANALYSIS OF THE GCM

In this GCM structure, light interacts with the graphene via evanescent field, which is confined tightly along the surface of the microfiber [35,36]. Such a graphene–light interaction not only reduces the GCM's thermal damage risk, but also dramatically enhances the effective action length of graphene. Accordingly, Fig. 3(a) shows the transmission of the GCM over the range of 1300–1600 nm. In comparison with pure microfiber with the same diameter, its loss is ~6 dB higher at 1550 nm, determined by the effective index of the GCM.

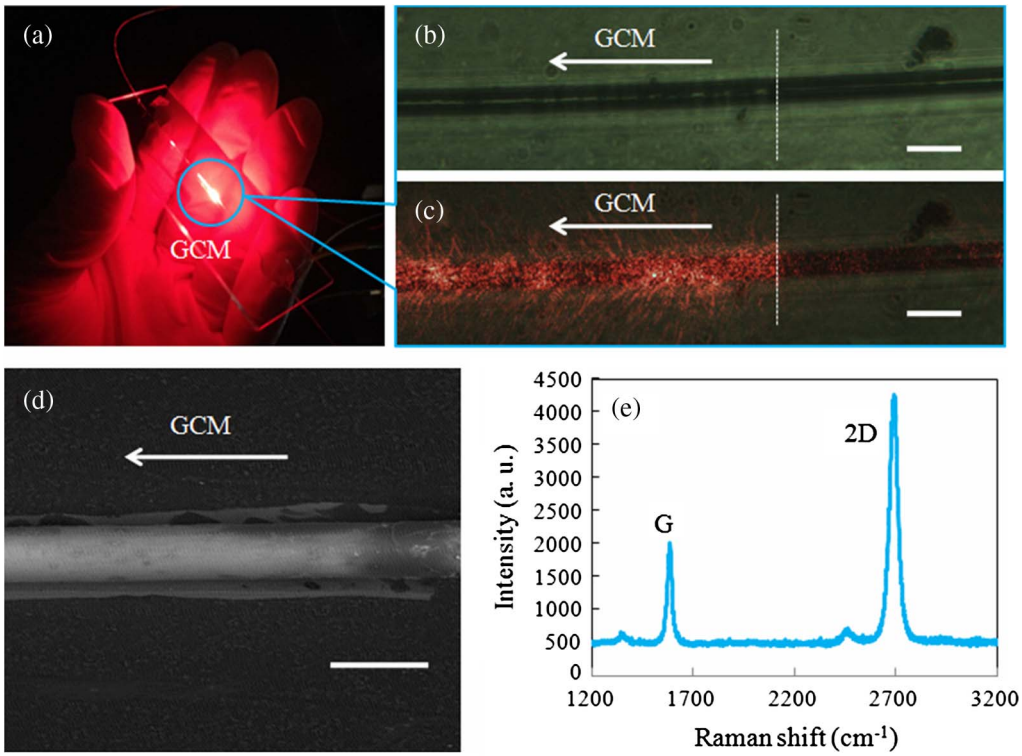

Fig. 2. (a) Dark-field photograph of the GCM; (b) optical micrograph of the GCM (bar, 10 μm); (c) under microscope, the graphene-induced surface scattering is obvious (bar, 10 μm); (d) SEM of the GCM (bar, 10 μm); (e) Raman spectrum of the GCM.

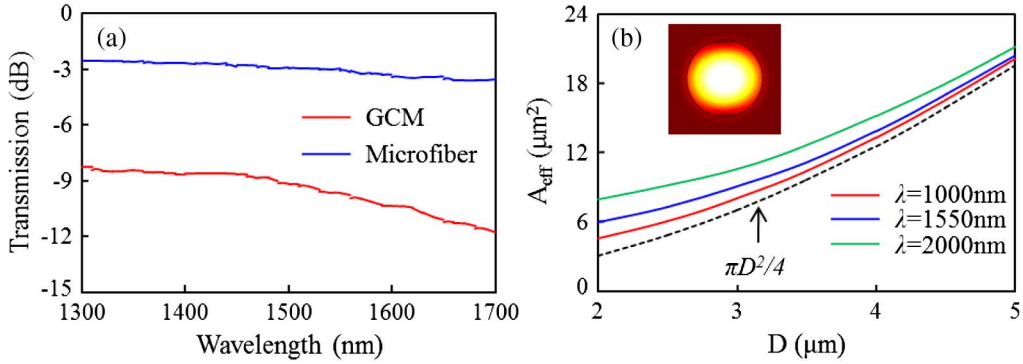

Fig. 3. (a) Transmission of the GCM (red) and the pure microfiber (blue); (b) correlation of the diameter and the effective mode area, in which the black dashed line shows the sectional area of the microfiber. Inset, mode distribution of the GCM with $D = 5$ μm at $\lambda = 1550$ nm (simulated by COMSOL).

Figure 3(b) shows the calculated correlations of diameter and effective field area ($D - A_{\text{eff}}$) for the fundamental mode in GCMs. Here the black dashed curve presents the area of the microfiber. Figure 3(b) illustrates that compared with common single mode fibers, the GCM with diameter of 5 μm has a thinner core, and a higher index difference between the core and the clad (for SMF, $n_{\text{core}} - n_{\text{clad}} < 0.02$, however for the microfiber, $n_{\text{core}} - n_{\text{clad}} \sim 0.46$), so that the light confinement A_{eff} along the GCM is dramatically smaller than a common SMF. For instance, when $D = 5$ μm and $\lambda = 1550$ nm, the A_{eff} of the GCM is calculated ~20.4 μm^2, while the A_{eff} of a SMF is ~78.5 μm^2. So, for the GCM, both the graphene and the microfiber contribute to the enhancement of nonlinear coefficient γ, referring $\gamma = n_2\omega/(cA_{\text{eff}})$, where n_2 is the nonlinear index of the GCM [37,38]. The value of γ for the GCM is calculated ~10^{10}, according to the third susceptibility of graphene $\chi_G^{(3)} = \sim 10^{-7}$ esu [24]. Figure 3(b), inset, shows the electric field distribution of the fundamental mode of the GCM with diameter of 5 μm. Moreover, as microfiber has anomalous dispersion while graphene cladding has normal dispersion over infrared spectrum, the chromatic dispersion of the GCM would be compensated and flatten. Considering the phase mismatch $\kappa = \Delta k + 2\gamma P$, where Δk is the dispersion contribution, it is helpful for the phase matching in FWM operation [39].

4. CASCADED FWM ON THE GCM

The experimental setup to demonstrate the GCM-based FWM is shown in Fig. 4. A CW laser with average power of 8.5 dBm was adopted as the signal, whose center wavelength could be tuned over a range of 1545–1555 nm. A high-power pulsed laser (B&A, M1042-1550) was used as the pump (FWHM 5 ns, repetition 1 kHz). The average power of the pump laser is tunable in range of 0–5.5 mW (corresponding to a peak power of 0–1100 W). First, the signal and the pump were coupled together by a direct coupler. Then the mixed light was launched in the GCM; after an attenuator, the output light of the GCM was collected by an optical spectral analyzer (OSA) (ANDO-AQ6317B) and a 1 GHz photon detector to be displayed on a fast oscilloscope (Agilent, Infiniium). In the setup, polarization controllers (PCs) were applied to optimize and maintain the polarization, and isolators (ISOs) were applied to reduce backscatter light.

The results of the FWM experiment are shown in Fig. 5. First of all, fixing the signal light at 1549.9 nm, we verified that the microfiber ($D = 5$ μm) without graphene cladding could not generate FWM, even though under the pump power of 3 mW, as shown in Fig. 5(a). Figure 5(a), inset, shows the locations of the CW light and the pump. Fixing the detuning to be 0.1 nm as well, the transmission spectra of the GCM under pump of 0.2 mW (200 MW/cm^2), 1 mW (1 GW/cm^2), and 3 mW (3 GW/cm^2) are shown in Fig. 5(b). As Fig. 5(b), inset, indicates, when the pump power was 0.2 mW, only one weak Stokes line of 1550.1 nm was generated. By increasing the pump power, cascaded FWM peaks were generated. When the pump power was 1 mW, four Stokes peaks and three anti-Stokes peaks were observed. Furthermore, when the pump power reached 3 mW, the cascaded Stokes and anti-Stokes peaks were filled in the range of approximately 1546–1558 nm. By adjusting the detuning $\Delta\lambda$, Fig. 5(c) presents the cascaded FWM spectra in the window of 1540–1560 nm. When $\Delta\lambda = 5$ nm, a generated Stokes line at 1555 nm was observed. Then, when $\Delta\lambda = 2$ nm, cascaded peaks distributed from 1546 to 1556 nm was obvious. Moreover, when $\Delta\lambda = 1$ nm, there were seven Stokes lines and four anti-Stokes lines. Meanwhile, via the oscilloscope, we monitored the output pulses in time-domain. It was observed that once turning on the CW light (signal), the FWM occurred, the power of the pulsed laser decreased by ~30%.

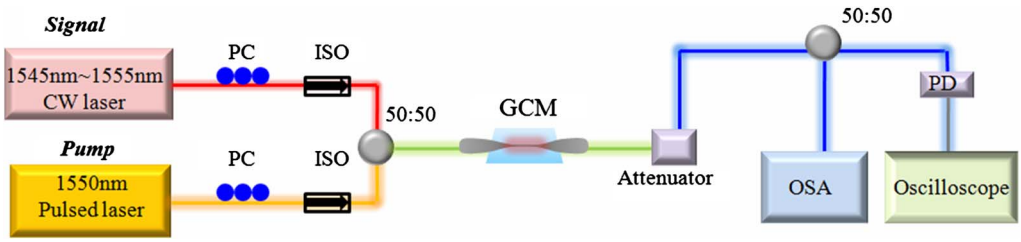

Fig. 4. Schematic diagram of the experimental setup.

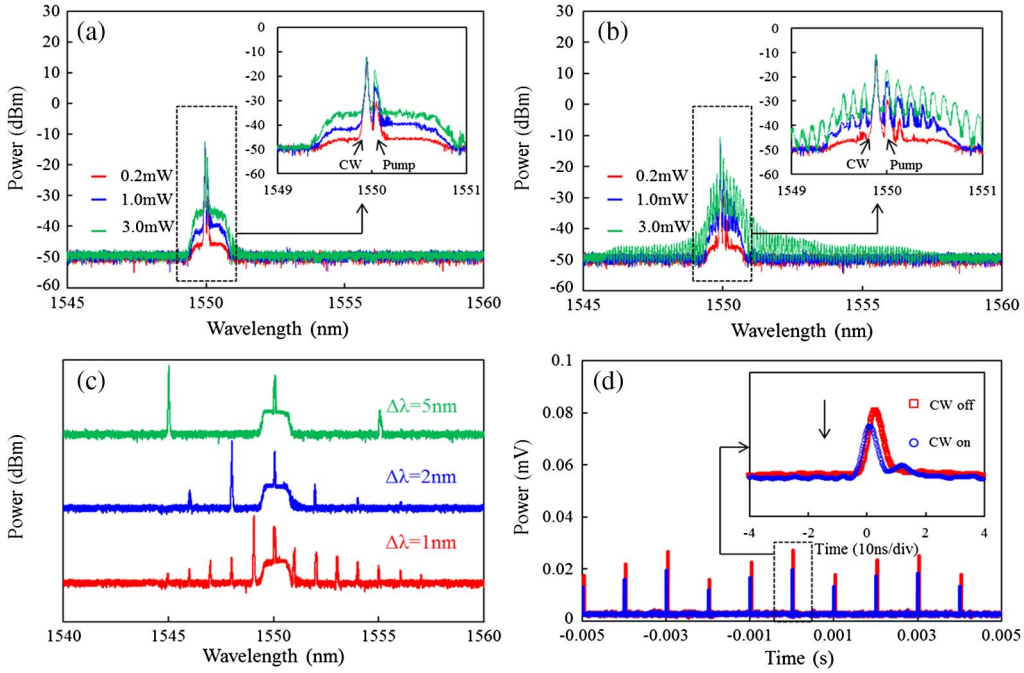

Fig. 5. (a) For the microfiber without graphene, no FWM was observed (1545–1560 nm). Inset, zoom-in figure with window of 1549–1551 nm; (b) spectra of the GCM under pump power of 0.2 mW (red), 1.0 mW (blue), and 3.0 mW (green). Inset, zoom-in figure with window of 1549–1551 nm; (c) spectra of cascaded FWMs for the detuning of 1 nm (red), 2 nm (blue), and 5 nm (green), respectively; (d) time profile of the transmitting light of the GCM, before CW launched (red boxes) and after CW launched (blue circles).

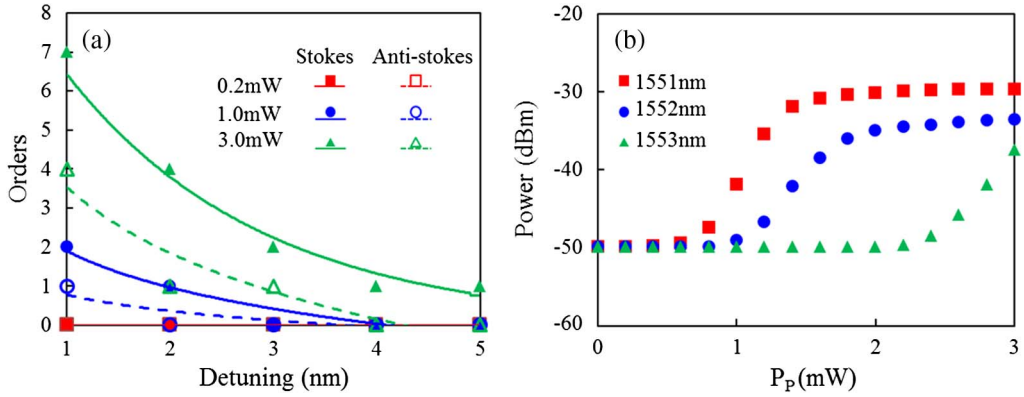

Fig. 6. (a) Correlation of the detuning and the orders of Stokes (solid curves) and anti-Stokes (dashed curves). Boxes, dots, and triangles correspond to 0.2 mW, 1 mW, and 3 mW, respectively; (b) correlation of the (P_P) and the power of first, second, and third Stokes peak, with fixing the detuning of 1 nm.

Accordingly, Fig. 6(a) summarizes the correlation of the detuning and the observed orders of Stokes band and anti-Stokes band. Here the dots are experimental samples and the curves are numerical fittings. When pump power was 0.2 mW, the nonlinear effects were too weak to observe; with the pump power increasing, cascaded FWM was generated; and when the pump power reached 3 mW, the spectra are as shown in Fig. 5. Figure 6(b) shows the relationship of the pump power (P_P) and the powers of the first-order (1551 nm), second-order (1552 nm), and third-order (1553 nm) Stokes line, with fixing the detuning to be 1 nm. With increasing P_P, the first-, second-, and third-order generated Stokes line appeared when P_P was 0.8 mW, 1 mW, and 2.2 mW, respectively. Then, when P_P increased to be 3 mW, the power of the first-order FWM light was saturated at approximately −30 dBm, with a conversion efficiency of approximately −20 dB. These Stokes bands and anti-Stokes bands could be broadened, and the conversion efficiency could be further improved, by optimizing the GCM structure, e.g. by decreasing the diameter of the microfiber to enhance the evanescent fields, increasing the length of the GCM to accumulate the nonlinear effects, utilizing the special fiber to adjust the dispersion, and so on.

5. CONCLUSIONS

In conclusion, by launching a CW light and a pulsed pump into a GCM hybrid waveguide, we demonstrated the cascaded FWM with tens of spanning lines. The span of the cascaded FWM is tunable by several nanometers, depending on the

detuning between the pulsed pump and the CW signal. Moreover, considering both the graphene and the microfiber contribute to the nonlinearity, the GCM-based FWM could be further optimized by adjusting the length of graphene, the diameter of microfiber, the index matching, and so on. This work may find applications in FWM-based frequency conversion, phase-sensitive amplifiers, comb filters, and all-optical regeneration.

ACKNOWLEDGMENTS

This work was supported by National Natural Science Foundation of China under Grants 61290312, 61107072, 61107073, and 61475032, and was also supported by Program for Changjiang Scholars and Innovative Research Team in Universities of China (PCSIRT) and the "111 Project" of China Education Ministry.

REFERENCES

1. F. Bonaccorso, Z. Sun, T. Hasan, and A. C. Ferrari, "Graphene photonics and optoelectronics," Nat. Photonics **4**, 611–622 (2010).
2. F. Abajo, "Graphene nanophotonics," Science **339**, 917–918 (2013).
3. Z. Q. Li, E. A. Henriksen, Z. Jiang, Z. Hao, M. C. Martin, P. Kim, H. L. Stormer, and D. N. Basov, "Dirac charge dynamics in graphene by infrared spectroscopy," Nat. Phys. **4**, 532–535 (2008).
4. Q. Bao, H. Zhang, Y. Wang, Z. Ni, Y. Yan, Z. Shen, K. Loh, and D. Tang, "Atomic-layer graphene as a saturable absorber for ultrafast pulsed lasers," Adv. Funct. Mater. **19**, 3077–3083 (2009).
5. B. Yao, Y. Wu, Z. Wang, Y. Cheng, Y. Rao, Y. Gong, Y. Chen, and Y. Li, "Demonstration of complex refractive index of graphene waveguide by microfiber-based Mach–Zehnder interferometer," Opt. Express **21**, 29818–29826 (2013).
6. M. Liu, X. Yin, E. Avila, B. Geng, T. Zentgraf, L. Ju, F. Wang, and X. Zhang, "A graphene-based broadband optical modulator," Nature **474**, 64–67 (2011).
7. W. Li, B. Chen, C. Meng, W. Fang, Y. Xiao, X. Li, Z. Hu, Y. Xu, L. Tong, H. Wang, W. Liu, J. Bao, and Y. Shen, "Ultrafast all-optical graphene modulator," Nano Lett. **14**, 955–959 (2014).
8. F. N. Xia, T. Mueller, Y. M. Lin, A. Garcia, and P. Avouris, "Ultrafast graphene photodetector," Nat. Nanotechnol. **4**, 839–843 (2009).
9. T. H. Han, Y. Lee, M. R. Choi, S. H. Woo, S. H. Bae, B. H. Hong, J. H. Ahn, and T. W. Lee, "Extremely efficient flexible organic light-emitting diodes with modified graphene anode," Nat. Photonics **6**, 105–110 (2012).
10. X. Gan, R. Shiue, Y. Gao, I. Meric, T. F. Heinz, K. Shepard, J. Hone, S. Assefa, and D. Englund, "Chip-integrated ultrafast graphene photodetector with high responsivity," Nat. Photonics **7**, 883–887 (2013).
11. Z. Sun, T. Hasan, F. Torrisi, D. Popa, G. Privitera, F. Wang, F. Bonaccorso, D. Basko, and A. C. Ferrari, "Graphene mode-locked ultrafast laser," ACS Nano **4**, 803–810 (2010).
12. X. He, Z. Liu, and D. Wang, "Wavelength-tunable, passively mode-locked fiber laser based on graphene and chirped fiber Bragg grating," Opt. Lett. **37**, 2394–2396 (2012).
13. B. Yao, Y. Wu, Y. Cheng, A. Zhang, Y. Gong, Y. Rao, Z. Wang, and Y. Chen, "All-optical Mach–Zehnder interferometric NH_3 gas sensor based on graphene/microfiber hybrid waveguide," Sens. Actuators B **194**, 142–148 (2014).
14. J. Kim, K. Chung, and C. Choi, "Thermo-optic mode extinction modulator based on graphene plasmonic waveguide," Opt. Express **21**, 15280–15286 (2013).
15. Q. Bao, H. Zhang, B. Wang, Z. Ni, C. H. Y. X. Lim, Y. Wang, D. Y. Tang, and K. P. Loh, "Broadband graphene polarizer," Nat. Photonics **5**, 411–415 (2011).
16. A. Cerqueira, J. Boggio, A. Rieznik, H. Figueroa, H. Fragnito, and J. C. Knight, "Highly efficient generation of broadband cascaded four-wave mixing products," Opt. Express **16**, 2816–2828 (2008).
17. Z. Tong, C. Lundstrom, P. A. Andrekson, C. J. McKinstrie, M. Karlsson, D. J. Blessing, E. Tipsuwannakul, B. J. Puttnam, H. Toda, and L. Grüner-Nielsen, "Towards ultrasensitive optical links enabled by low-noise phase-sensitive amplifiers," Nat. Photonics **5**, 430–436 (2011).
18. X. Gai, D. Choi, S. Madden, and B. Davies, "Polarization-independent chalcogenide glass nanowires with anomalous dispersion for alloptical processing," Opt. Express **20**, 13513–13521 (2012).
19. J. Kakande, R. Slavik, F. Parmigiani, A. Bogris, D. Syvridis, L. Nielsen, R. Phelan, P. Petropoulos, and D. J. Richardson, "Multilevel quantization of optical phase in a novel coherent parametric mixer architecture," Nat. Photonics **5**, 748–752 (2011).
20. H. Yang, X. Feng, Q. Wang, H. Huang, W. Chen, A. Wee, and W. Ji, "Giant two-photon absorption in bilayer graphene," Nano Lett. **11**, 2622–2627 (2011).
21. R. Wu, Y. Zhang, S. Yan, F. Bian, W. Wang, X. Bai, X. Lu, J. Zhao, and E. Wang, "Purely coherent nonlinear optical response in solution dispersions of graphene sheets," Nano Lett. **11**, 5159–5164 (2011).
22. N. Kumar, J. Kumar, C. Gerstenkorn, R. Wang, H. Chiu, A. Smirl, and H. Zhao, "Third harmonic generation in graphene and few-layer graphite films," Phys. Rev. B **87**, 121406 (2013).
23. S. Hong, J. Dadap, N. Petrone, P. Yeh, J. Hone, and R. Osgood, "Optical third-harmonic generation in graphene," Phys. Rev. X **3**, 021014 (2013).
24. E. Hendry, P. Hale, J. Moger, and A. Savchenko, "Coherent nonlinear optical response of graphene," Phy. Rev. Lett. **105**, 097401 (2010).
25. Z. Zhang and P. L. Voss, "Full-band quantum-dynamical theory of saturation and four-wave mixing in graphene," Opt. Lett. **36**, 4569–4571 (2011).
26. B. Xu, A. Martinez, and S. Yamashita, "Mechanically exfoliated graphene for four-wave-mixing-based wavelength conversion," IEEE J. Photon. Technol. Lett. **24**, 1792–1794 (2012).
27. Z. Luo, M. Zhou, D. Wu, C. Ye, J. Weng, J. Dong, H. Xu, Z. Cai, and L. Chen, "Graphene-induced nonlinear four-wave-mixing and its application to multiwavelength *Q*-switched rare-earth-doped fiber lasers," IEEE J. Lightwave Technol. **29**, 2732–2739 (2011).
28. T. Gu, N. Petrone, J. F. McMillan, A. Zande, M. Yu, G. Lo, D. Kwong, J. Hone, and C. W. Wong, "Regenerative oscillation and four-wave mixing in graphene optoelectronics," Nat. Photonics **6**, 554–559 (2012).
29. H. Zhou, T. Gu, J. McMillan, N. Petrone, A. Zande, J. Hone, M. Yu, G. Lo, D. Kwong, G. Feng, S. Zhou, and C. Wong, "Enhanced four-wave mixing in graphene-silicon slow-light photonic crystal waveguides," Appl. Phys. Lett. **105**, 091111 (2014).
30. Y. Wu, B. Yao, Y. Cheng, Y. Rao, X. Zhou, B. Wu, and K. S. Chiang, "Four-wave mixing in a microfiber attached onto a graphene film," IEEE J. Photon. Technol. Lett. **20**, 249–252 (2014).
31. G. P. Agrawal, *Nonlinear Fiber Optics*, 4th ed. (Elsevier, 2009).
32. Z. Wang, Y. Chen, P. Li, X. Hao, J. Liu, R. Huang, and Y. Li, "Flexible graphene-based electroluminescent devices," ACS Nano **5**, 7149–7154 (2011).
33. G. K. Lim, Z. L. Chen, J. Clark, R. G. S. Goh, W. H. Ng, H. W. Tan, R. H. Friend, P. K. H. Ho, and L. L. Chua, "Giant broadband nonlinear optical absorption response in dispersed graphene single sheets," Nat. Photonics **5**, 554–560 (2011).
34. E. Ferreira, M. Moutinho, F. Stavale, M. Lucchese, R. Capaz, C. Achete, and A. Jorio, "Evolution of the Raman spectra from single-, few-, and many-layer graphene with increasing disorder," Phys. Rev. B **82**, 125429 (2010).
35. P. Wang, G. Brambilla, M. Ding, Y. Semenova, Q. Wu, and G. Farrell, "High-sensitivity, evanescent field refractometric sensor based on a tapered, multimode fiber interference," Opt. Lett. **36**, 2233–2235 (2011).
36. L. Tong, J. Lou, and E. Mazur, "Single-mode guiding properties of subwavelength-diameter silica and silicon wire waveguides," Opt. Express **12**, 1025–1035 (2004).
37. A. Gorbach, A. Marini, and D. V. Skryabin, "Graphene-clad tapered fiber: Effective nonlinearity and propagation losses," Opt. Lett. **38**, 5244–5247 (2013).
38. Y. H. Li, Y. Y. Zhao, and L. J. Wang, "Demonstration of almost octave-spanning cascaded four-wave mixing in optical microfibers," Opt. Lett. **37**, 3441–3443 (2012).
39. H. Zhang, D. Tang, L. Zhao, Q. Bao, K. P. Loh, B. Lin, and S. Tjin, "Compact graphene mode-locked wavelength-tunable erbium-doped fiber lasers: from all anomalous dispersion to all normal dispersion," Laser Phys. Lett. **7**, 591–596 (2010).